Journal of Alloys and Compounds, 191 (1993) 291–295
JALCOM 520

Study of the microstructure of a new hexagonal Sm_2Fe_{17} phase with the Th_2Ni_{17}-type structure

L. L. He, H. Q. Ye, X. R. Xu and J. F. He
Laboratory of Atomic Imaging of Solids, Institute of Metal Research, Academia Sinica, Shenyang 110015 (China)

(Received May 13, 1992; in final form September 9, 1992)

Abstract

A study of the microstructure of the rapidly solidified $Sm_2Fe_{17}N_{3-x}$ alloy was carried out using transmission electron microscopy. A new hexagonal Sm_2Fe_{17} phase, with space group $P6_3/mmc$ and lattice parameters $a=0.854$ and $c=0.828$ nm, was found. This hexagonal phase is metastable and can only be formed during rapid solidification. The high resolution image also identified many 2:17H domains inside the 2:17R phase. Large-angle trigrain boundaries with a 120° rotation relationship between any two c axes were often formed in the alloy.

1. Introduction

The high performance permanent magnet based on the $Nd_2Fe_{14}B$ phase has been studied extensively since it was discovered in 1983. The search for new iron-rich rare earth intermetallic compounds with interesting hard magnetic properties has also been initiated. Recently, Coey *et al.* [1, 2] have reported a new permanent magnetic alloy $Sm_2Fe_{17}N_{3-x}$, which demonstrates improved magnetic properties compared with $Nd_2Fe_{14}B$ compounds. This new magnetic alloy has a coercivity H_{ci} of 3.5 T and an energy product $(BH)_{max}$ of 12.5 MGOe [3]. The $Sm_2Fe_{17}N_{3-x}$ alloys are manufactured firstly by nitrogenating Sm_2Fe_{17} alloy powders and then by extruding them into magnets [1–3]. There are at least three methods for the preparation of Sm_2Fe_{17} alloy powders: (1) normal melting; (2) melt spinning; (3) mechanical alloying. The powders prepared by different methods may show different microstructures and this may affect the nitrogenation process and even the magnetic properties. Hence a study of the microstructure of the Sm_2Fe_{17} alloy is necessary to improve the nitrogenation process and the magnetic properties.

The Sm_2Fe_{17} phase is a rare earth–transition metal(R–TM) compound and R_2TM_{17} compounds, especially R–Co and R–Fe alloys, show good magnetic properties [5–8]. The R_2Fe_{17} alloys exhibit two kinds of structure: a rhombohedral lattice (Th_2Zn_{17}-type) with a space group $R\bar{3}m$ and a hexagonal lattice (Th_2Ni_{17}-type) with a space group $P6_3/mmc$. They are made up by the alternate stacking of two kinds of atomic planes: the 3636 network of Fe atoms and mixture networks (which are composed of the 3^6 network of Fe dumbbells surrounded by a 6^3 network of Fe atoms and a large 6^3 network of Sm atoms). The difference between them is the stacking sequence, *i.e.* ABCABC for the rhombohedral structure and ABAB for the hexagonal structure; their c axes have a relationship $c_{Hex}=2/3c_{Rhom}$ as shown in Fig. 1. The lattice parameters vary with the element R and are in the range $a=0.845$–0.857 nm and $c=1.232$–1.244 nm for the rhombohedral structure and $a=0.839$–848 nm and $c=0.826$–0.830 nm for the hexagonal structure [9, 10]. For the R_2Fe_{17} compounds, some only exhibit the Th_2Zn_{17} structure if R is lighter than gadolinium, *e.g.* Ce_2Fe_{17} and Pr_2Fe_{17}, and some only exhibit the Th_2Ni_{17} structure if R is heavier than dysprosium, *e.g.* Ho_2Fe_{17} and Er_2Fe_{17}. Others possess

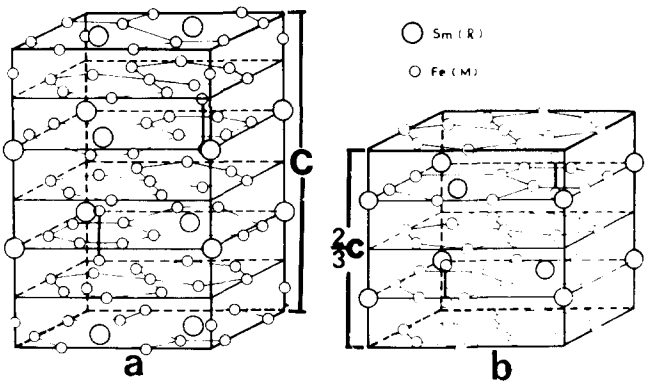

Fig. 1. Unit cell of the two structures for the R_2TM_{17} alloy: (a) rhombohedral Th_2Zn_{17} structure; (b) hexagonal Th_2Ni_{17} structure. They can be considered as the alternate arrangement of two types of atomic planes: the 3636 network of Fe atoms and a mixture network (composed of the 3^6 network of Fe atom dumbbells surrounded by the 6^3 network of Fe atoms and a large 6^3 network of Sm atoms).

0925-8388/93/$6.00

the Th_2Ni_{17} structure at high temperature (or in cast) and the Th_2Zn_{17} structure at low temperature, *e.g.* Gd_2Fe_{17} and Dy_2Fe_{17}. The addition of certain alloying elements, *e.g.* carbon, can affect this experimental rule and produce a new phase [11–13]. However, Sm_2Fe_{17} only exhibits the Th_2Zn_{17} rhombohedral structure and no Th_2Ni_{17} hexagonal structure has been reported in cast or quenching conditions [5, 8, 10].

In this paper, we concentrate on the microstructure of rapidly solidified Sm_2Fe_{17} alloy. Its effect on the magnetic properties of the $Sm_2Fe_{17}N_{3-x}$ alloy is also discussed.

2. Experimental details

The bulk Sm_2Fe_{17} alloy was prepared by melting the pure Sm and Fe elements (99.99%) under an argon atmosphere in a non-consumable arc furnace. The alloy was remelted at least four times in order to achieve homogeneity. Excess Sm was used to compensate the loss of Sm during melting, so that the amount of free b.c.c. Fe could be limited to a minimum. Rapidly solidified alloy ribbons were prepared using a vacuum melt-spinning machine under an argon atmosphere with a surface velocity of about 31.5 m s^{-1}, and these ribbons were then converted to powders. Some thinner ribbons, about 20–40 μm thick, were chosen to prepare the samples used in this study. The thin films for transmission electron microscopy were prepared firstly by electro-polishing in a twin-jet machine using a 5% $HClO_4$–ethanol electrolyte at −30 °C and 30 V, followed by ion-beam thinning with a low angle (7–10°) for 1–2 h. A large-angle double-tilting experiment was performed using a JEM-200CX electron microscope for electron diffraction (ED) analyses. High resolution electron microscopy (HREM) observations was carried out using a JEOL-2000EXII electron microscope with a point-to-point resolution of about 0.21 nm.

3. Results

Figure 2 shows the ED patterns taken from the two different phases in this alloy. Figure 2(a) is the characteristic ED pattern of the main phase. ED analysis demonstrates that this pattern is the [11$\bar{2}$0] zone ED pattern of the rhombohedral Sm_2Fe_{17} phase, which has a Th_2Zn_{17} structure (2:17R). Since there are some (001) microtwin structures in the 2:17R phase, which can be considered as rhombohedral Sm_2Fe_{17} variants with a different stacking sequence ACBACB and the reflection condition $-h+k-l=3n$, the 1$\bar{1}$01 and 2$\bar{2}$02 spots have weak intensity, *i.e.* all spots with $-h+k\pm l=3n$, have reflections [12, 14, 15]. The ED

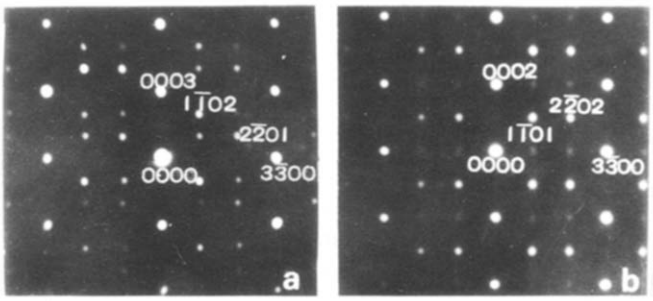

Fig. 2. [11$\bar{2}$0] ED patterns taken from the 2:17R phase (a) and the 2:17H phase (b).

TABLE 1. Diffraction intensity of the 2:17H phase for electron diffraction

Index	Structure factor	Index	Structure factor
0000	–	1$\bar{1}$00	0.5
0001	0.0	1$\bar{1}$01	4.9
0002	4.9	1$\bar{1}$02	11.1
0003	0.0	1$\bar{1}$03	22.4
0004	100.0	1$\bar{1}$04	11.4
2$\bar{2}$00	2.1	3$\bar{3}$00	8.9
2$\bar{2}$01	6.3	3$\bar{3}$01	0.2
2$\bar{2}$02	7.6	3$\bar{3}$02	37.4
2$\bar{2}$03	20.8	3$\bar{3}$03	6.1
2$\bar{2}$04	9.1	3$\bar{3}$04	22.2

pattern shown in Fig. 2(b) cannot be indexed using any ED patterns of the 2:17R phase. The fact that the spots with $l=2n$ along the [000l]* direction have strong reflection implies that this phase should belong to the hexagonal structure. This ED pattern can be indexed as the [11$\bar{2}$0] zone pattern of a hexagonal lattice with lattice constants $a_{Hex}=a_{2:17R}$ and $c_{Hex}=2/3c_{2:17R}$. This relationship just satisfies the co-relation of the two structures in the R_2TM_{17} alloys shown in Figs. 1(a) and 1(b). Therefore this hexagonal phase has the Th_2Ni_{17}-type structure.

Analysis of the diffraction intensity confirms these conclusions. Table 1 shows the structure factors of the diffraction spots calculated using the atomic coordinates of the Th_2Ni_{17} structure with Th ≡ Sm and Ni ≡ Fe. On the whole the calculated intensities of the spots agree with the experimental results in Fig. 2(b), except the spots (000l) with $l=4n+2$. According to kinematic theory, these spots should show weaker intensities than the spots (000l) with $l=4n$ because there is a 3636 network of Fe atoms between every A and B network shown in Fig. 1(b). In fact, the same disagreement also exists in the ED pattern of the 2:17R phase (Fig. 2(a)). This disagreement, however, can be explained by the double diffraction effect. The dynamic calculation proves that the diffraction intensities of the (0002) and (0004) spots are almost the same at a certain thickness as

shown in Fig. 3. Hence we have identified a new hexagonal Sm_2Fe_{17} phase with the Th_2Ni_{17} structure (2:17H) in the rapidly solidified Sm_2Fe_{17} alloy with the lattice parameters $a = 0.854$ nm and $c = 0.828$ nm.

Figure 4(a) shows the HREM image of the 2:17H phase viewed along the [11$\bar{2}$0] direction in which each bright dot represents a column of the alternate mixture of Fe atoms and Fe atomic dumbbells. The unit cell is outlined in the centre and the c axis is indicated at the top right of the figure. In Fig. 4(a), we can observe the stacking sequence ABAB along the [0001] direction, as marked in the P region. Figure 4(b) shows the corresponding projection of the unit cell and Fig. 4(c) shows the calculated image along the [11$\bar{2}$0] direction with a defocus value of about 90.0 nm and a thickness of 11.7 nm. Each dot on the experimental image corresponds to the Fe dumbbells in the projected structure. In comparison with the HREM image of the 2:17R phase [14, 15], our HREM observation and a series of corresponding image simulations along this direction prove that the new phase is the hexagonal Sm_2Fe_{17} phase with the Th_2Ni_{17}-type structure. Moreover, the simulated image in Fig. 4(b) is in the same region as the pronounced dynamic diffraction effect in Fig. 3. Therefore our image simulation and diffraction intensity calculations are self-consistent and the 2:17H phase is identified in the Sm_2Fe_{17} alloy.

The 2:17H phase disappears after annealing the rapidly solidified ribbons at 500–600 °C for about 5–10 min. This demonstrates that the 2:17H phase is metastable.

Figure 5 shows the [11$\bar{2}$0] HREM image at the site where the 2:17H domains are formed in the 2:17R phase. The projected unit cell of 2:17R indicated by R and that of 2:17H indicated by H are also marked (note that the unit cell of 2:17H has a shifted origin point compared with that of Fig. 4). A composite [11$\bar{2}$0] ED pattern from the 2:17H and 2:17R phases is shown in the inset. The pattern shows the common 3$\bar{3}$00 spots and the overlapped spots of $0002_{2:17H}$ and $0003_{2:17R}$. The large arrows indicate the ED spots of 2:17H and the small arrows indicate those of 2:17R. In comparison with Figs. 1(a) and 1(b), the 2:17R and 2:17H phases are of the same atomic configuration in the (0001) plane but have different stacking order along the [0001] direction. When the phase transformation from the $SmFe_5$ phase to the Sm_2Fe_{17} phase takes place during rapid solidification, the substitution of the Fe dumbbells for Sm atoms in the (0001) plane is almost complete, but the stacking sequence along the [0001] direction is not totally rhombohedral and therefore some 2:17H domains coexist with the 2:17R phase. In Fig. 5, a multitude of domain structures are illustrated. The small arrows in Fig. 5 indicate the 2:17H domains

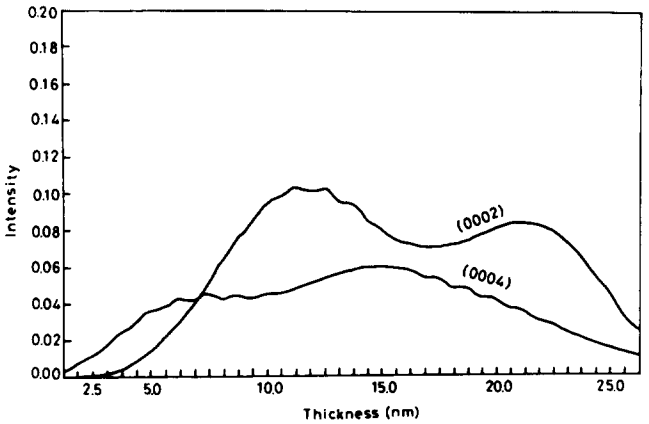

Fig. 3. Intensity curves of the 0002 and 0004 reflections which show that the two reflections have almost the same intensities beyond a thickness of about 8.0 nm.

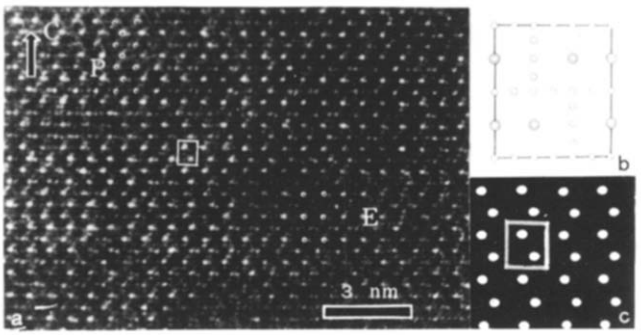

Fig. 4. [11$\bar{2}$0] HREM image of the 2:17H phase: (a) experimental image; (b) atomic projection cell along this direction: (c) simulated image under the conditions of a defocus value of 90.0 nm and a thickness of about 11.7 nm.

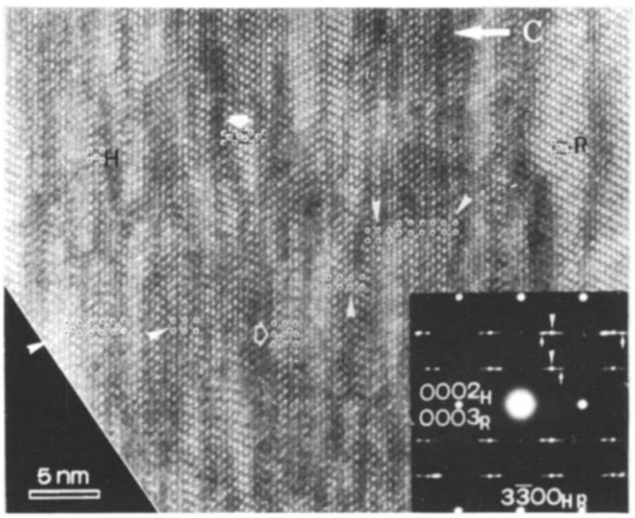

Fig. 5. The [11$\bar{2}$0] HREM image shows that many 2:17H domains are formed inside the 2:17R phase (small arrows); large filled arrow, coexisting domains of the 2:17R and 2:17H phase; large open arrow, 2:17H domain with stacking faults. The inset shows the corresponding ED pattern composed of the [11$\bar{2}$0] ED patterns of the 2:17R and 2:17H phase.

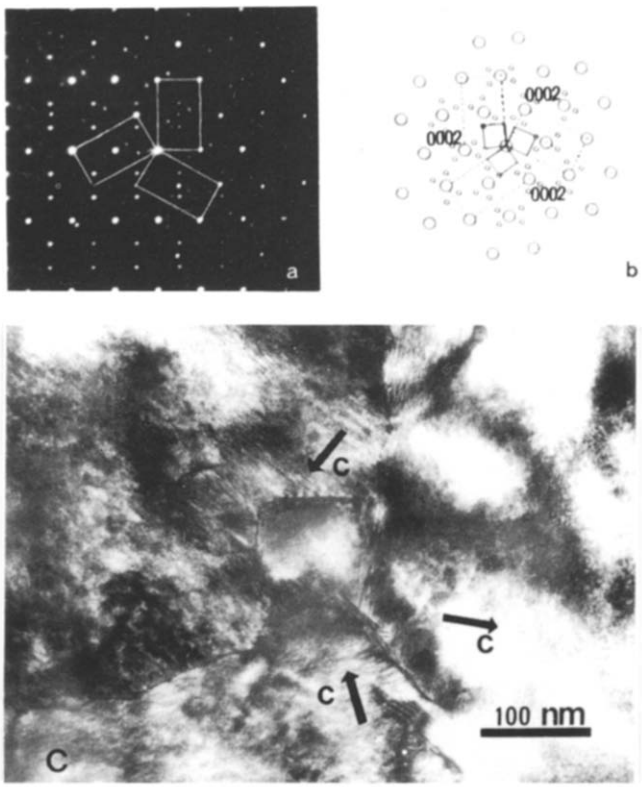

Fig. 6. The 120° large-angle trigrain boundaries: (a) and (b) ED pattern and schematic indexing respectively; (c) bright field image.

with the stacking sequence ABAB. The large filled arrow shows the coexistence of the 2:17H and 2:17R domains with the stacking sequence ACABCAC. Some stacking faults in the 2:17H domain are also shown. For example, the double hexagonal structure with the stacking sequence ABACA has been given in the region marked by the open arrow.

The 2:17H phase grains often form large-angle trigrain boundaries where their c axes have a 120° rotation relationship as shown in Fig. 6. Figure 6(a) demonstrates the $[11\bar{2}0]$ zone ED pattern taken from such trigrain boundaries, which can be indexed as three sets of $[11\bar{2}0]$ zone ED patterns with a 120° rotation relationship. Figure 6(b) shows the schematic indexing of Fig. 6(a). Many diffraction streaks along the c^* axes in Fig. 6(a) imply that there are many stacking faults in every grain. The bright field image in Fig. 6(c) demonstrates one of these 120° trigrain boundaries. In each grain there are many stacking fault streaks which are mostly normal to the c axis and the angles between these streaks are exactly 120° or 60°. This result matches well with the conclusion from the ED analysis in Fig. 6(a).

4. Discussion

In general, the R_2TM_{17} intermetallic phases exhibit magnetic properties. Their magnetic anisotropies determine whether or not they can be used as permanent magnetic materials. There are two kinds of magnetic anisotropy: easy plane and easy c axis; only the latter can be used to produce permanent magnets. All the R_2Fe_{17} compounds, whether hexagonal or rhombohedral exhibit easy plane anisotropy; however, the magnetic anisotropy of the rhombohedral Sm_2Fe_{17} compound can be changed to easy c axis anisotropy by nitrogenation ($Sm_2Fe_{17}N_{3-x}$ exhibits easy c axis anisotropy). It is not clear whether hexagonal Sm_2Fe_{17} and its nitride possess easy c axis or easy plane anisotropy. If they possess easy plane anisotropy, their existence may be detrimental to the magnetic properties of the $Sm_2Fe_{17}N_{3-x}$ alloy. Although annealing could eliminate this phase, heat treatment may also lead to an increased grain size of the 2:17R phase and larger grains are detrimental to the nitrogenation process.

The hexagonal Sm_2Fe_{17} phase forms large-angle grain boundaries as shown in Fig. 6, and these trigrain boundaries may be detrimental to the residual magnetism B_r and the energy product $(BH)_{max}$.

In the Sm–Fe alloy family, $SmFe_{12}$ and $SmFe_7$ phases also exist. Their structures can be derived directly from the $SmFe_5$ structure by substitution of Fe atomic dumbbells for certain Sm atoms. The 2:17R and 2:17H phases exhibit the same substitution in the (0001) planes, but the other two structures possess different substitution. Because there are no $SmFe_{12}$ and $SmFe_7$ phases in this alloy, we can conclude that the substitution is nearly perfect on each (0001) plane under rapid cooling conditions. However, the positions of the Fe atom dumbbells are not so regular along the [0001] direction. At one extreme 2:17R is generated and at the other 2:17H is formed. At intermediate stages many stacking faults are produced in both phases.

5. Conclusions

(1) In rapidly solidified Sm_2Fe_{17} alloy the hexagonal Sm_2Fe_{17} phase with the Th_2Ni_{17} structure and space group $P6_3/mmc$ has been determined for the first time. Its unit cell parameters are $a = 0.854$ nm and $c = 0.828$ nm.

(2) This phase is metastable and exhibits many defects. The formation of these defects is due to the varied substitution of the Fe atom dumbbells for Sm atoms in the (0001) planes and such change also alters the stacking sequence of the basal planes. The 2:17H phase can be formed by rapid solidification and eliminated by annealing treatment.

(3) Under rapid solidification, the 2:17H domains can coexist with the main 2:17R phase.

(4) The 2:17H phase often forms large-angle trigrain boundaries with a 120° rotation relationship between the *c* axes.

Acknowledgments

The authors acknowledge helpful discussions with Dr. Zhang Zhi Dong.

References

1 J. M. D. Coey, H. Sun and Y. Otani, *J. Appl. Phys., 69* (1990) 2737.
2 J. E. D. Coey and H. Sun, *J. Magn. Magn. Mater., 87* (1990) L125.
3 Q. Wang, W. Liu, X. G. Zhao, L. B. Wang, G. Y. Geng, T. Zhao, Z. D. Zhang, C. H. Wu, X. K. Sun, H. Q. Ye and Y. C. Chang, *Proc. 2nd Int. Symp. Phys. Magn. Mater., Beijing, July, 1992,* p. 608.
4 K. Schnitzke, L. Schultz and J. Wecker, *Appl. Phys. Lett., 57* (1990) 2853.
5 K. H. J. Buschow, *J. Less-Common Met., 11* (1966) 204–208.
6 K. H. J. Buschow and A. S. Van der Goot, *J. Less-Common Met., 14* (1968) 323–328.
7 Y. Khan and B. Mueller, *J. Less-Common Met., 32* (1973) 39–45.
8 Y. Khan, *Acta Crystallogr. Sect. B, 29* (1973) 2502–2507.
9 W. B. Pearson, *The Crystal Chemistry and Physics of Metals and Alloys,* Wiley-Interscience, New York, 1992, pp. 643–661.
10 H. Sun, J. M. D. Coey, Y. Otani and D. P. F. Hurley, *J. Phys. Condens. Matter, 2* (1990) 6465.
11 W. Coene, F. Hakkens, T. H. Jacobs, D. B. Mooij and K. H. J. Buschow, *J. Less-Common Met., 157* (1990) 255.
12 W. Coene, F. Hakkens, T. H. Jacobs and K. H. J. Buschow, *Philos. Mag. A, 63* (1991) 185.
13 W. Coene, F. Hakkens, T. H. Jacobs and K. H. J. Buschow, *J. Solid State Chem., 92* (1991) 191.
14 Z. L. Xie, L. L. He and H. Q. Ye, in H. Hashimoto, T. Ko, K. H. Kuo and K. Ogawa (eds.), *Fifth Chinese–Japanese Seminar on Electron Microscopy, Xin Jiang, September 1990,* Komiyama Printing Co., Tokyo, 1990, pp. 129–132.
15 L. L. He, J. H. Li and H. Q. Ye, *Electron Microscopy, 4* (1990) 996–997.